**38th Fluid Dynamics Conference and Exhibit
**
23 - 26 June 2008, Seattle, Washington

AIAA 2008-3993

Improvement of the WENO Scheme Smoothness Estimator

Yiqing Shen* Gecheng Zha†
Miami Wind^{TM}
Dept. of Mechanical and Aerospace Engineering
University of Miami
Coral Gables, Florida 33124
E-mail: yqshen@miami.edu, gzha@miami.edu

Abstract

This paper has analyzed the weights of the 5th order WENO (weighted essentially non-oscillatory) scheme suggested by Jiang and Shu and a modified smoothness estimator is suggested to improve the accuracy. Several numerical tests are presented to demonstrate the accuracy and robustness of the new scheme.

1 Introduction

For the numerical simulation of complicated flowfields, such as shock wave/boundary layer interaction and shock wave/vortex interaction, it is required that the numerical schemes have the ability of shock capturing and fine-scale feature capturing. Due to the capability of capturing shock waves and the uniformly high order accuracy in the smooth regions, the WENO (weighted essentially non-oscillatory) schemes have been widely used to study these flows[1, 2, 3, 4, 5, 6].

The WENO scheme concept was firstly proposed by Liu et al[7] and then greatly improved by Jiang and Shu[1]. WENO schemes are based on ENO (essentially non-oscillatory) schemes[8, 9], but use a convex combination of all candidate stencils instead of the smoothest one in the ENO schemes. The WENO schemes have more advantages over their ENO counterparts. For example, they approach high order accuracy in smooth regions and have better convergence rate due to the smoother numerical flux used.

Jiang and Shu[1] analyzed and modified the 5th WENO scheme proposed by Liu et al[7] and suggested a new way of measuring the smoothness of a numerical solution. Thus a WENO scheme with the optimal $(2r-1)$th order accuracy rather than $(r+1)$th order is obtained. Henrick et al[10] pointed out that the original smoothness indicators of Jiang and Shu fails to improving the order of WENO scheme at a critical point, where the first derivatives is zero. A mapping function is proposed by Henrick et al[10] to obtain the optimal order near critical points. Borges et al[11] devised a new set of WENO weights that satisfies the necessary and sufficient conditions for fifth-order convergence proposed by Henrick et al[10] and enhances the accuracy at critical points.

Ideally, the smoothness estimators $IS_k(k=0,\cdots,r-1)$ should be uniformly small in the smooth flow regions and the magnitudes should be about the same (the difference is $O(\Delta x^2)$). Under these condition, the weights ω_k will approach the optimum weights C_k as $\omega_k = C_k + O(\Delta x^{r-1})$, and result in the 5th order accuracy. Unfortunately, this is usually not true in the practical calculations due to the non-uniformity of

---

[*] Research Scientist, AIAA Member

[†] Associate Professor, AIAA Senior Member, Director of Miami Wind^{TM}

flowfields and mesh size. There always exists a significant difference between the smoothness estimators IS_k even in the smooth regions[12]. Very often, this difference is large enough to deviate the weights ω_k from the optimum weights C_k and hence increase the numerical dissipation. One way to cure this problem is to increase the ε value as suggested in[12].

In this paper, a different approach to improve the smoothness estimators has been proposed to balance the difference between the maximum and minimum values of IS_k to obtain better accuracy. This paper mainly compares the numerical results of the smoothness estimators of Jiang and Shu [1] and the newly suggested one. For the smoothness estimators of Borges et al[11], the accuracy can be also further improved with the new treatment, especially for the solution with high wave number or shock waves. Some comparisons with the scheme of Borges et al[11] are also given in this paper.

2 Analysis and Improvement of the 5th WENO scheme

The following hyperbolic conservation law is usually accepted as a model equation for Euler equation.

$$\frac{\partial u}{\partial t} + \frac{\partial f}{\partial x} = 0 \tag{1}$$

with the initial condition

$$u(x,0) = u_0(x) \tag{2}$$

Its general semi-discrete form can be written as

$$\frac{du_j}{dt} = -\frac{1}{\Delta x}(h_{j+1/2} - h_{j-1/2}) \tag{3}$$

The flux function $f(u)$ can be split into two parts, i.e., $f(u) = f^+(u) + f^-(u)$ with $df^+(u)/du \geq 0$ and $df^-(u)/du \leq 0$. And then the numerical flux function $h_{j+1/2}$ is obtained by

$$h_{j+1/2} = h^+_{j+1/2} + h^-_{j+1/2} \tag{4}$$

As in Ref.[1], only $h^+_{j+1/2}$ will be described in this paper, and the superscript "+″ will be dropped. The $h^-_{j+1/2}$ is evaluated following the symmetric rule about $x_{j+1/2}$.

2.1 The fifth-order WENO scheme

The numerical flux of the fifth-order WENO ($r = 3$)scheme of Jiang and Shu[1] is:

$$h_{i+1/2} = \omega_0 q_0 + \omega_1 q_1 + \omega_2 q_2$$

where ω_0, ω_1 and ω_2 are the weights, and the q_0, q_1 and q_2 are the 3rd order accuracy reconstruction of the variables in three different stencils. They are determined as the following,

$$q_0 = \frac{1}{3}f_{j-2} - \frac{7}{6}f_{j-1} + \frac{11}{6}f_j$$

$$q_1 = -\frac{1}{6}f_{j-1} + \frac{5}{6}f_j + \frac{1}{3}f_{j+1}$$

$$q_2 = \frac{1}{3}f_j + \frac{5}{6}f_{j+1} - \frac{1}{6}f_{j+2}$$

and

$$\omega_k = \frac{\alpha_k}{\alpha_0 + \cdots + \alpha_{r-1}}, \tag{5}$$

$$\alpha_k = \frac{C_k}{(\varepsilon + IS_k)^p}, \quad k = 0, \cdots, r-1 \tag{6}$$

where C_k are the optimal weights, which give 5th order central difference scheme, with the following values:

$$C_0 = 0.1, \quad C_1 = 0.6, \quad C_2 = 0.3$$

and $p = 2$. The IS_k are the smoothness estimators[1] determined as

$$IS_k = \sum_{l=1}^{r-1} \int_{x_{j-1/2}}^{x_{j+1/2}} h^{2l-1} (p_k^{(l)})^2 dx \tag{7}$$

where $h = \Delta x$. $p_k(x)$ is the interpolation polynomial on stencil $S_k = (x_{j+k-r+1}, \cdots, x_{j+k})$, $p_k^{(l)}$ is the lth-derivative of $p_k(x)$. For $r = 3$, Eq.(7) gives

$$IS_0 = \frac{13}{12}(f_{j-2} - 2f_{j-1} + f_j)^2 + \frac{1}{4}(f_{j-2} - 4f_{j-1} + 3f_j)^2$$

$$IS_1 = \frac{13}{12}(f_{j-1} - 2f_j + f_{j+1})^2 + \frac{1}{4}(f_{j-1} - 4f_j + 3f_{j+1})^2$$

$$IS_2 = \frac{13}{12}(f_j - 2f_{j+1} + f_{j+2})^2 + \frac{1}{4}(f_j - 4f_{j+1} + 3f_{j+2})^2$$

The ε in Eq.(6) is introduced to avoid the denominator becoming zero. Jiang and Shu's numerical tests indicate that the results are not sensitive to the choice of ε, as long as it is in the range of 10^{-5} to 10^{-7}. In their paper, ε is taken as 10^{-6}.

If

$$IS_k = D(1 + O(\Delta x^{r-1})), k = 0, \cdots, r-1,$$

then

$$\omega_k = C_k + O(\Delta x^{r-1})$$

where D is independent of r and k, and the accuracy of the WENO achieves $2r-1$ order.

Borges et al [11] devised a new set of WENO weights ω_k that satisfies the sufficient condition for fifth-order convergence:

$$\omega_k^{\pm} - C_k = O(\Delta x^3)$$

by defining the new smoothness indicators IS_k^z as

$$IS_k^z = \frac{IS_k + \varepsilon}{IS_k + \tau_5 + \varepsilon}, \ k = 0, 1, 2$$

where

$$\tau_5 = |IS_0 - IS_2|.$$

In reality, due to the non-uniformity of flow solution or finite grid size, there always exist variation between IS_k or IS_k^z . Sometimes, the variation, even though small, is enough to make ω_k largely deviate from C_k.

In order to study the effects of IS_k variation on ω_k(the conclusion is also applicable to IS_k^z), we assume that the influence of ε is negligible without losing generality, i.e. $\varepsilon = 0$, and

$$max(IS_0, \cdots, IS_{r-1}) = (1 + \phi) min(IS_0, \cdots, IS_{r-1}) \tag{8}$$

$$min(IS_0, \cdots, IS_{r-1}) \neq 0, \phi \geq 0$$

hence,

$$\phi = \frac{max(IS_0, \cdots, IS_{r-1})}{min(IS_0, \cdots, IS_{r-1})} - 1$$

and, define the ratio R as

$$R = \frac{min^2(IS_0, \cdots, IS_{r-1})}{max^2(IS_0, \cdots, IS_{r-1})} = \frac{1}{(1+\phi)^2}$$

According to Eq. (6), the closer the R to unity, the more uniform the IS_k are, and hence the closer the ω_k to C_k, which will give the WENO scheme the minimum dissipation.

The ratio R vs ϕ is plotted in Fig. 1 as the curve of $A = 0$(A will be defined later). It can be seen that the R starts to deviate from 1 when ϕ is equal to 10^{-2}, which means that the $max(IS_0, \cdots, IS_{r-1})$ is only 1% greater than $min(IS_0, \cdots, IS_{r-1})$. In a discretized system, it is desirable to treat such a small difference of the solution as a smooth solution with near central differencing to minimize numerical dissipation.

2.2 Improvement of IS_k

Based on above analysis, a modified IS'_k is proposed to replace the IS_k,

$$IS'_k = R_0 A min(IS_0, \cdots, IS_{r-1}) + IS_k \tag{9}$$

where

$$R_0 = \frac{min(IS_0, \cdots, IS_{r-1})}{max(IS_0, \cdots, IS_{r-1}) + \varepsilon'} \tag{10}$$

In Eq. (10), ε' is introduced to avoid the denominator becoming zero. In this paper, ε' is taken as 10^{-10}. In Eq. (9), A is a constant parameter and will be discussed more later.

Corresponding to IS'_k, a new weight function α'_k is defined as

$$\alpha'_k = \frac{C_k}{(\varepsilon + IS'_k)^p}, \ \ k = 0, \cdots, r-1 \tag{11}$$

and

$$\omega_k = \frac{\alpha'_k}{\alpha'_0 + \cdots + \alpha'_{r-1}}, \tag{12}$$

Clearly, the following conclusions apply:

$$\begin{cases} if \ A \rightarrow 0 \ or \ min(IS_0, ..., IS_{r-1}) \rightarrow 0, & \alpha'_k \rightarrow \alpha_k, \ the \ original \ 5th \ order \ WENO \ achived \\ if \ A \rightarrow \infty \ and \ min(IS_0, ..., IS_{r-1}) \neq 0, & \omega_k \rightarrow C_k, \ the \ 5th \ order \ with \ optimal \ weights \ achieved \end{cases} \tag{13}$$

Similarly, the ratio R' is defined as

$$R' = \frac{min^2(IS'_0, \cdots, IS'_{r-1})}{max^2(IS'_0, \cdots, IS'_{r-1})} = (\frac{\frac{A}{1+\phi} + 1}{\frac{A}{1+\phi} + 1 + \phi})^2$$

Clearly, if A equals 0, then R' becomes R, i.e., $R' = R = min^2(IS_0, \cdots, IS_{r-1})/max^2(IS_0, \cdots, IS_{r-1})$.

Fig. 1 shows the ratio R' with different A vs ϕ. It can be seen that, when A is increased, the range of R' close to 1 is also increased. When $R' = 1$, the WENO scheme has the optimum weights with minimum numerical dissipation. In our numerical experiments, the solutions with discontinuity are still essentially non-oscillatory with A up to 100. Moreover, R_0^β with $\beta \geq 0$ can be used to replace R_0 in Eq.(9), and then A can be even a larger number. In this paper, $\beta = 1$ and $A = 10$ are used.

To demonstrate the different behavior of the new smoothness estimators in smooth regions, near critical points and near discontinuities, we compute the weights ω_0, ω_1, and ω_2 for the function

$$f = \begin{cases} sin^2(2\pi x), & 0 \leq x \leq 0.5 \\ 1 - sin^2(2\pi x), & x \geq 0.5 \end{cases} \tag{14}$$

at points $x_{j+1/2} = (j + 1/2)\Delta x$ with $\Delta x = 1/40$.

Fig. 2 is the distribution of the weights ω_0 and $\omega_1(\omega_2 = 1 - \omega_0 - \omega_1$ is omitted in the picture). It can be seen that in smooth regions, the weights computed with Eq. (12) are closer to optimal values than those with original smoothness estimator. Near the discontinuity, the two estimators behave similarly.

2.3 Numerical Examples

In this paper, the 4th order Runge-Kutta-type method[13] is used for the time integration. For the ordinary differential equation

$$\frac{du}{dt} = L(u)$$

the 4th order Runge-Kutta method is

$$\begin{array}{l} u^{(1)} = u^n + \frac{1}{2}\Delta t L(u^n) \\ u^{(2)} = u^n + \frac{1}{2}\Delta t L(u^{(1)}) \\ u^{(3)} = u^n + \Delta t L(u^{(2)}) \\ u^{(n+1)} = \frac{1}{3}(-u^n + u^{(1)} + 2u^{(2)} + u^{(3)}) + \frac{1}{6}\Delta t L(u^{(3)}) \end{array} \tag{15}$$

where $L(u)$ is the operator of spatial discretization, Δt is the temporal interval.

2.3.1 Linear transport equation

As in Ref.[1], the linear transport equation is used to test the accuracy of WENO schemes.

$$\frac{\partial u}{\partial t} + \frac{\partial u}{\partial x} = 0, \ -1 < x < 1 \tag{16}$$

$$u(x, 0) = u_0(x), \ periodic$$

(1) Initial solution $u_0(x) = sin(\pi x)$

In Table 1, the errors and accuracy of the WENO schemes at $t = 1$ are compared with those of the fifth order central differencing scheme. It can be seen that the present scheme with IS'_k and $A = 10$ gives the uniformly 5th order accuracy similar to the central differencing. The original WENO scheme does not achieve the expected 5th order accuracy on the coarse grid ($N = 20$).

The better accuracy with IS'_k can be explained from Figs. 3-13. Fig. 3 shows that, near the critical points with large variation of gradient, there is a significant difference among IS_k, which result in the ratio $R = min^2(IS_0, IS_1, IS_2)/max^2(IS_0, IS_1, IS_2)$ deviated from 1. Hence, the numerical dissipation is increased.

Fig. 4 shows that the difference among IS'_k is much smaller. The $R' = min^2(IS'_0, IS'_1, IS'_2)/max^2(IS'_0, IS'_1, IS'_2)$ is essentially kept at value of 1 as shown in Fig. 13, whereas the R value determined by IS_k is largely shifted from 1.

Table 1: Accuracy on $u_t + u_x = 0$ with $u_0(x) = sin(\pi x)$, t=1

ε	N	L_∞ error	L_∞ order	L_1 error	L_1 order
Original IS_k	10	0.295802E-01	—-	0.159099E-01	—-
	20	0.145516E-02	4.345	0.738828E-03	4.429
	40	0.459126E-04	4.986	0.222080E-04	5.056
	80	0.147518E-05	4.960	0.690047E-06	5.008
	160	0.435897E-07	5.081	0.216551E-07	4.994
	320	0.127744E-08	5.093	0.677434E-09	4.998
	640	0.365857E-10	5.126	0.210608E-10	5.007
present IS'_k $(A = 10)$	10	0.888788E-02	—-	0.553838E-02	—-
	20	0.259687E-03	5.097	0.163234E-03	5.084
	40	0.838436E-05	4.953	0.489118E-05	5.061
	80	0.272698E-06	4.942	0.152698E-06	5.001
	160	0.842200E-08	5.017	0.478615E-08	4.996
	320	0.261418E-09	5.010	0.149906E-09	4.997
	640	0.793321E-11	5.042	0.468975E-11	4.998
Central-5	10	0.480067E-02	—-	0.294034E-02	—-
	20	0.156312E-03	4.941	0.970183E-04	4.922
	40	0.497645E-05	4.973	0.310914E-05	4.964
	80	0.156236E-06	4.993	0.983828E-07	4.982
	160	0.488801E-08	4.998	0.309373E-08	4.991
	320	0.152795E-09	5.000	0.969814E-10	4.996
	640	0.481115E-11	4.989	0.303622E-11	4.997

In Fig. 13, it can be seen that there is a large difference between the weights obtained by IS_k and IS'_k. The weights obtained by IS'_k remain at the optimum values, whereas those obtained by the original IS_k deviate significantly from the optimum values and are also not smooth.

The accuracy using IS'_k is thus higher than the original Jiang and Shu's scheme due to less dissipation. Even though both WENO schemes have 5th order accuracy on fine grid, the errors of present scheme are about 1/4 of those of the original one as indicated in Table 1.

(2) Initial solution $u_0(x) = sin^4(\pi x)$

The comparisons of errors and accuracy-order is given in Table 2. For this testing case, the similar conclusions as in example (1) can be observed except on the mesh size N=80. The accuracies of both schemes on $N = 80$ degrade to 3rd order. This is caused by the very large difference between the IS_k as shown in Fig. 5. For example, at the point $x_{j+1/2} = -0.0375$, IS_0 is about 1000 times greater than IS_2. So the point is treated as a "discontinuity" point. With refined grid points, the difference become smaller, and the accuracy order is restored to 5th order. Table 2 shows that the error using the suggested IS'_k is nearly one-order of magnitude lower than that of the original scheme.

(3) Initial solution $u_0(x) = sin(4\pi x)$

This cases is used to test the accuracy of the present WENO scheme with increased wave number. The comparisons of errors and accuracy-order is given in Table 3. Again, the original scheme can not obtain 5th order accuracy on the coarse grids such as $N = 40$ and $N = 80$. The present scheme achieves the similar order of accuracy as the 5th order central differencing scheme. Similar to the conclusions drawn in above two examples, the error of present scheme is about 1/4 of that of the original one.

The treatment suggested in this paper is also applied to the smoothness estimator of Borges et al[11]. Fig. 6 shows that the smoothness estimators of Borges et al[11] with the new treatment improves the

Table 2: Accuracy on $u_t + u_x = 0$ with $u_0(x) = sin^4(\pi x)$, t=1

ε	N	L_∞ error	L_∞ order	L_1 error	L_1 order
Original IS_k	20	0.106962E+00	—-	0.489555E-01	—-
	40	0.890319E-02	3.587	0.363465E-02	3.752
	80	0.169913E-02	2.390	0.477658E-03	2.928
	160	0.681324E-04	4.640	0.148159E-04	5.011
	320	0.176045E-05	5.274	0.386343E-06	5.261
	640	0.287460E-07	5.936	0.908032E-08	5.411
present IS'_K $(A = 10)$	20	0.699319E-01	—-	0.374434E-01	—-
	40	0.373100E-02	4.228	0.176131E-02	4.410
	80	0.467889E-03	2.995	0.130560E-03	3.754
	160	0.130532E-04	5.164	0.337469E-05	5.274
	320	0.345754E-06	5.239	0.872902E-07	5.274
	640	0.702410E-08	5.621	0.234445E-08	5.219
Central-5	20	0.518129E-01	—-	0.330531E-01	—-
	40	0.245848E-02	4.397	0.150600E-02	4.456
	80	0.831144E-04	4.887	0.506742E-04	4.893
	160	0.264444E-05	4.974	0.159382E-05	4.991
	320	0.830058E-07	4.994	0.498661E-07	4.998
	640	0.259680E-08	4.998	0.155890E-08	4.999

Table 3: Accuracy on $u_t + u_x = 0$ with $u_0(x) = sin(4\pi x)$, t=1

ε	N	L_∞ error	L_∞ order	L_1 error	L_1 order
Original IS_k	20	0.848441E+00	—-	0.532581E+00	—-
	40	0.803166E-01	3.401	0.552895E-01	3.268
	80	0.453987E-02	4.145	0.286306E-02	4.271
	160	0.168606E-03	4.751	0.889742E-04	5.008
	320	0.540834E-05	4.962	0.278472E-05	4.998
	640	0.165847E-06	5.027	0.870152E-07	5.000
present IS'_K $(A = 10)$	20	0.717390E+00	—-	0.450057E+00	—-
	40	0.302780E-01	4.566	0.208502E-01	4.432
	80	0.903444E-03	5.067	0.672305E-03	4.955
	160	0.316272E-04	4.836	0.198621E-04	5.081
	320	0.103186E-05	4.938	0.616205E-06	5.010
	640	0.327245E-07	4.979	0.192318E-07	5.002
Central-5	20	0.410170E+00	—-	0.260707E+00	—-
	40	0.190679E-01	4.427	0.121625E-01	4.422
	80	0.625103E-03	4.931	0.399214E-03	4.929
	160	0.199056E-04	4.973	0.126431E-04	4.981
	320	0.624942E-06	4.993	0.397008E-06	4.993
	640	0.195521E-07	4.998	0.124312E-07	4.997

accuracy slightly for this case.

(4) Initial solution

$$u_0(x) = \begin{cases} \frac{1}{6}(G(x,\beta,z-\delta)+G(x,\beta,z+\delta)+4G(x,\beta,z)), & -0.8 \leq x \leq -0.6, \\ 1, & -0.4 \leq x \leq -0.2, \\ 1-|10(x-0.1)|, & 0 \leq x \leq 0.2, \\ \frac{1}{6}(F(x,\alpha,\alpha-\delta)+F(x,\alpha,\alpha+\delta)+4F(x,\alpha,a)), & 0.4 \leq x \leq 0.6, \\ 0, & otherwise \end{cases} \tag{17}$$

As in Ref.[1], the constants are taken as $a = 0.5$, $z = -0.7$, $\delta = 0.005$, $\alpha = 10$, and $\beta = log2/36\delta^2$. The solution contains a smooth combination of Gaussians, a square wave, a sharp triangle wave, and a half ellipse.

The results at $t = 4$ with 200 grid points are shown in Fig. 7. From the zoomed plots of Figures 8 and 9, it can be seen that, for the resolution of critical point and discontinuities, the result computed by the present scheme is significantly more accurate than the original WENO scheme.

Again, the proposed new treatment is used for the scheme of Borges et al and the results at $t = 8$ with 200 grid points are shown in Figs. 10-12. It can be seen that, for the resolution of critical point and discontinuities, the substantially more accurate result is obtained by the new treatment.

2.3.2 Nonlinear Transport Equation

The nonlinear transport equation can be written as

$$\frac{\partial u}{\partial t} + u\frac{\partial u}{\partial x} = 0, \ 0 \leq x \leq 2\pi$$

with initial and boundary conditions

$$u_0(x) = 0.3 + 0.7sin(x), \ 0 \leq x \leq 2\pi, \ periodic$$

The Lax-Friedrichs splitting method is used, in which $f^{\pm} = \frac{1}{2}(f(u) \pm au)$, $f(u) = \frac{1}{2}u^2$, and $a = max_u|f'(u)|$. Fig. 14 shows the results at $t = 2$ with grid number of $N = 80$. It can be seen that, near the two ends of the shock, the solution calculated by the present scheme is closer to the discontinuous points than those of the original scheme.

Fig. 15 shows the results of the scheme of Borges et al and the scheme with new treatment at $t = 2$ with grid number of $N = 40$. The more accurate solution near the shock wave is also obtained by the scheme with the new treatment.

2.3.3 Viscous Burgers Equation

The viscous Burgers equation is used to test the accuracy and the capability of capturing steady state shock. The viscous Burgers equation is written as

$$\frac{\partial u}{\partial t} + u\frac{\partial u}{\partial x} = \frac{1}{Re}\frac{\partial^2 u}{\partial x^2}, \ a \leq x \leq b \tag{18}$$

with initial conditions

$$\begin{cases} u(a) = tanh(-aRe/2), \\ u(b) = tanh(-bRe/2). \end{cases} \tag{19}$$

The steady state solution of Eq. (18) and (19) is $u(x) = tanh(-xRe/2)$. At $x = 0$, the shock is formed when the Re number is large. In our computation, $a = -1$, $b = 1$, and $Re = 1000$ are taken, and the grid number is $N = 80$. The central differencing scheme is used for the second-order viscous derivative. The results are shown in Fig. 16. Again, both schemes capture the shock discontinuity very well.

Fig. 17 is the comparison of smoothness indicators of Borges et al with new treatment. The grid number is $N = 40$. The solution is also improved by the new treatment.

2.3.4 1D Shock Wave Tube, Sod Problem

The governing equation for the 1D shock tube is the one-dimensional Euler equations,

$$\frac{\partial \mathbf{U}}{\partial t} + \frac{\partial \mathbf{F}}{\partial x} = 0 \tag{20}$$

where

$$\mathbf{U} = \begin{bmatrix} \rho \\ \rho u \\ \rho e \end{bmatrix} \mathbf{F} = \begin{bmatrix} \rho u \\ \rho u^2 + p \\ u(\rho e + p) \end{bmatrix}, \, p = (\gamma - 1)(\rho e - \rho u^2/2), \, \gamma = 1.4.$$

The initial condition is

$$(\rho, u, p) = \begin{cases} (1.0, 0.0, 1.0), & x \leq 7.5, \\ (0.125, 0.0, 0.1), & x > 7.5. \end{cases} \tag{21}$$

In this case, the Roe's Riemann solver is used. The grid points is $N = 200$. Figs. 18 and 19 give the density and velocity distribution. Both the original and the new scheme capture the shock and contact surface very well.

2.3.5 1D Shock Wave Tube, Shu-Osher Problem

This problem is governed by the one-dimensional Euler equations (20) with following initial condition:

$$(\rho, u, p) = \begin{cases} (3.857143, 2.629369, 10.3333), & when\ x < -4, \\ (1 + \varepsilon sin(5x), 0.0, 1.0), & when\ x \geq -4. \end{cases} \tag{22}$$

where, $\varepsilon = 0.2$. This case represents a Mach 3 shock wave interacting with a sine entropy wave[9]. The results at time $t = 1.8$ are plotted in Figs. 20 and 21. The “exact” solutions are the numerical solutions of the original WENO-5 scheme with grid points of $N = 8000$. For this case, it can be seen in Fig. 21 that the present WENO scheme resolves the profile significantly better than the original WENO scheme, which smears the profile due to high dissipation.

2.3.6 Two-dimensional Linear Conservation law with variable coefficients

The governing equation is

$$\frac{\partial u}{\partial t} + \frac{\partial(-yu)}{\partial x} + \frac{\partial(xu)}{\partial y} = 0, \ -1 \leq x, y \leq 1. \tag{23}$$

and the periodic boundary conditions are used. The initial condition is chosen as the characteristic function of a circle with radius 0.5 as shown in Fig. 22. The problem represents a solid body rotation[14, 15]. The results at $t = 2$ in a 100×100 points grid are shown in Figs. 23-24. Note that in Fig. 24, the exact solution at $x = -0.52$ is $u(-0.52, y) = 0$. It can be seen that, in the strong shock regions, the present WENO scheme has the similar results as the original WENO scheme; in the smooth regions, the present WENO scheme obtains more accurate solution.

2.3.7 Two-dimensional Shock Reflection Problem

The governing equation is two-dimensional Euler equations

$$\frac{\partial \mathbf{U}}{\partial t} + \frac{\partial \mathbf{E}}{\partial x} + \frac{\partial \mathbf{F}}{\partial y} = 0 \tag{24}$$

where

$$\mathbf{U} = \begin{bmatrix} \rho \\ \rho u \\ \rho v \\ \rho e \end{bmatrix}, \mathbf{E} = \begin{bmatrix} \rho u \\ \rho u^2 + p \\ \rho uv \\ u(\rho e + p) \end{bmatrix}, \mathbf{F} = \begin{bmatrix} \rho v \\ \rho uv \\ \rho v^2 + p \\ v(\rho e + p) \end{bmatrix},$$

$p = (\gamma - 1)(\rho e - \rho(u^2 + v^2)/2)$, $\gamma = 1.4$.

The initial condition is

$$(\rho, u, v, p) = \begin{cases} (1.0, 2.9, 0.0, 0.714286), & \textit{ahead of the incident shock}, \\ (1.69997, 2.61934, -0.50633, 1.52819), & \textit{behind the incident shock}. \end{cases} \tag{25}$$

The incident shock angle is 29^o and a free stream Mach number is 2.9. The computational domain is $[4 \times 1]$ with uniform grid of 121×41 points. The Steger-Warming's flux vector splitting method[16] is applied to this case. Fig. 25 shows the pressure contours computed by the present WENO scheme. Fig. 26 shows the comparison of the results of the two WENO schemes. Both results agree well with each other for this case.

2.3.8 Two-dimensional Shock Vortex Interaction

The governing equations and the flux splitting method are the same as in section (2.3.7).

The problem is taken from Ref.[1]. It describes the interaction between a stationary shock and a vortex. The computational domain is taken to be $[0, 2] \times [0, 1]$. A stationary Mach 1.1 shock is positioned at $x = 0.5$ and normal to the x-axis. Its left state is $(\rho, u, v, p) = (1, 1.1\sqrt{\gamma}, 0, 1)$. A small vortex is superimposed to the flow left to the shock and is centered at $(x_c, y_c) = (0.25, 0.5)$. The vortex is described as a perturbation to the velocity (u, v), temperature $(T = p/\rho)$, and entropy $(S = ln(p/\rho^\gamma))$ of the mean flow and denoted by the tilde values:

$$\tilde{u} = \varepsilon \tau e^{a(1-\tau^2)} sin\theta$$

$$\tilde{v} = -\varepsilon \tau e^{a(1-\tau^2)} cos\theta$$

$$\tilde{T} = -\frac{(\gamma - 1)\varepsilon^2 e^{2a(1-\gamma^2)}}{4a\gamma}$$

$$\tilde{S} = 0$$

where $\tau = r/r_c$ and $r = \sqrt{(x - x_c)^2 + (y - y_c)^2}$, ε indicates the strength of the vortex, a controls the decay rate of the vortex, and r_c is the critical radius for which the vortex has the maximum strength. As in the Refs. [1, 5], $\varepsilon = 0.3$, $r_c = 0.05$, and $a = 0.204$ are adopted in this paper. The uniform grid of 251×101 is used. The time step is taken as follows[17]:

$$\Delta t = \delta \Delta_x \Delta_y, \ with \ \delta_x = \frac{\Delta x}{max_{i,j}(|u_{i,j}| + c_{i,j})}, \ \delta_y = \frac{\Delta y}{max_{i,j}(|v_{i,j}| + c_{i,j})} \tag{26}$$

Figs. 27 and 28 are the pressure contours at $t = 0.35$ and $t = 0.60$. Figs. 29 and 30 are the comparisons of the pressure between the present and the original scheme along the center line at $y = 0.5$. Fig. 29 shows that the new scheme has the sharper shock profile. Fig. 30 indicates that the new scheme achieves lower vortex core pressure due to smaller dissipation.

3 Conclusions

This paper analyzes the smoothness estimators of the Jiang-Shu's 5th order WENO scheme. It is observed that the small variation between the smoothness estimators can significantly increase the numerical dissipation of the WENO scheme. A modified smoothness estimators is suggested to reduce the variation and make the weights close to the optimum value in smooth regions, which will give the minimum numerical dissipation. The value of the parameter A at $10 \sim 100$ is recommended to improve the accuracy in the smooth region and maintain the sensitivity to shock or contact surface discontinuities. This new treatment to improve the smoothness estimators is applicable to the original smoothness estimators of Jiang and Shu[1], and to the recent smoothness estimators of Borges et al[11]. The numerical results indicate that using the modified smooth estimators has improved the accuracy due to the reduced numerical dissipation.

4 Acknowledgment

This work is partially supported by AFOSR Grant F49620-03-1-0253 monitored by Dr Fariba Fahroo, by ARO grant 56827-RT-ISP monitored by Lt Col. R. Jefferies at AFOSR and J. Haire at ARO, and by Miami Wind^{TM} at University of Miami.

References

[1] G.S. Jiang, and C.W. Shu, "Efficient implementation of weighted ENO schemes," *J.Comput.Phys.*, vol. 126, pp. 202–228, 1996.

[2] S. Pirozzoli, "Conservative hybrid compact-WENO schemes for shock-turbulence interaction," *J.Comput.Phys.*, vol. 178, pp. 81–117, 2002.

[3] B. Sjogreen and H.C. Yee, "Grid convergence of high order methods for multiscale complex unsteady viscous compressible flows," *Journal of Computational Physics*, vol. 185, pp. 1–26, 2003.

[4] M. Latini, O. Schilling, W.S. Don, "Effects of WENO flux reconstruction order and spatial resolution on reshocked two-dimensional Richtmyer-Meshkov instability," *Journal of Computational Physics*, vol. 221, pp. 805–836, 2007.

[5] Y.Q. Shen and G.W. Yang, "Hybrid finite compact-WENO schemes for shock calculation," *Interational Journal for Numerical Methods in Fluids*, vol. 53, pp. 531–560, 2007.

[6] Y.Q. Shen, G.C. Zha, and B.Y. Wang, "Improvement of the stability and accuracy of implicit WENO scheme for transonic flows." Submitted to AIAA J., 2007.

[7] X.D. Liu, S. Osher, and T. Chan, "Weighted essentially non-oscillatory schemes," *J.Comput.Phys.*, vol. 126, pp. 200–212, 1994.

[8] A. Harten, B. Engquist, S. Osher, and S. Chakravarthy, "Uniformly High Order Essentially Non-Oscillatory Schemes, III," *Journal of Computational Physics*, vol. 71, pp. 231–303, 1987.

[9] C.-W. Shu and O. Osher, "Efficient Implementation of Essentially Non-Oscillatory Shock Capturing Schemes, II," *Journal of Computational Physics*, vol. 83, pp. 32–78, 1989.

[10] A.K. Henrick, T.D. Aslam, J.M. Powers, "Mapped weighted essentially non-oscillatory schemes:Achiving optimal order near critical points," *J.Comput.Phys.*, vol. 208, pp. 206–227, 2005.

[11] R. Borges, M. Carmona, B. Costa and W.S. Don, "An improved weighted essentially non-oscillatory scheme for hyperbolic conservation laws," *Journal of Computational Physics*, vol. 227, pp. 3191–3211, 2008.

[12] Y.Q. Shen, G.C. Zha, and B.Y. Wang, "Improvement of the stability and accuracy of implicit WENO scheme for transonic flows." AIAA-paper 2007-4431, Submitted to AIAA J., 2008.

[13] C.-W. Shu and O. Osher, "Efficient Implementation of Essentially Non-Oscillatory Shock Capturing Schemes," *Journal of Computational Physics*, vol. 77, pp. 439–471, 1988.

[14] B. Cockburn, C.W. Shu, "Nonlinearly stable compact schemes for shock calculations," *SIAM Journal on Numerical Analysis*, vol. 31, pp. 607–627, 1994.

[15] Y.Q. Shen, G.W. Yang, Z. Gao, "High-resolution finite compact difference schemes for hyperbolic conservation laws," *J.Comput.Phys.*, vol. 216, pp. 114–137, 2006.

[16] J. Steger and R. Warming, "Flux Vvector Splitting of the Inviscid Gasdynamic Equations with Application to Finite-Difference Methods," *Journal of Computational Physics*, vol. 40, pp. 263–293, 1981.

[17] Z.J. Wang and R.F. Chen, "Optimized weighted essentially non-oscillatory schemes for linear waves with discontinuity," *J.Comput.Phys.*, vol. 174, pp. 381–404, 2001.

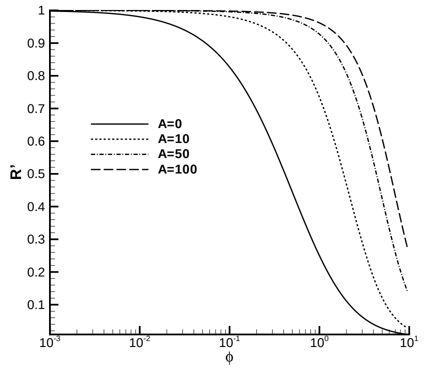

Figure 1: The variation of the ratio R' vs ϕ

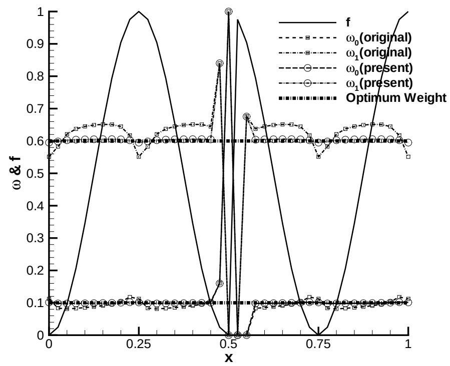

Figure 2: Comparison of the two smoothness estimators

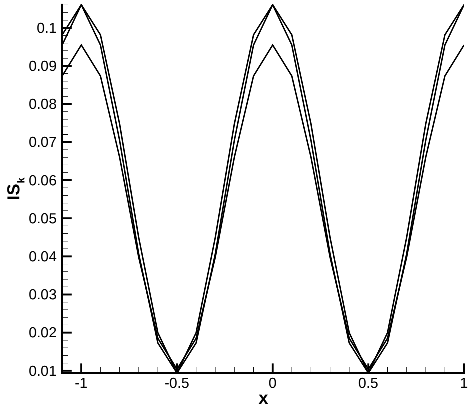

Figure 3: IS_k distribution of $sin(\pi x)$, N=20

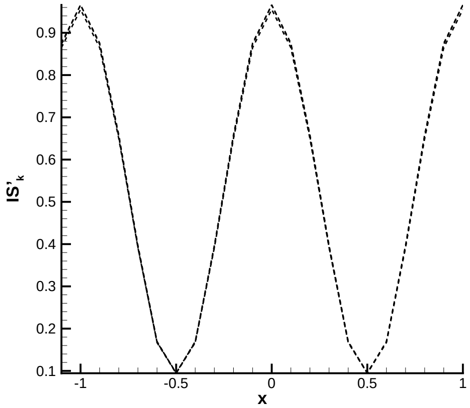

Figure 4: IS'_k distribution of $sin(\pi x)$, N=20

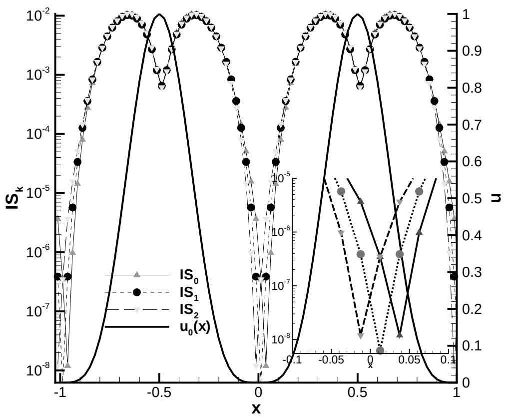

Figure 5: Distribution of IS_k, $u_0(x) = sin^4(\pi x)$, N=80

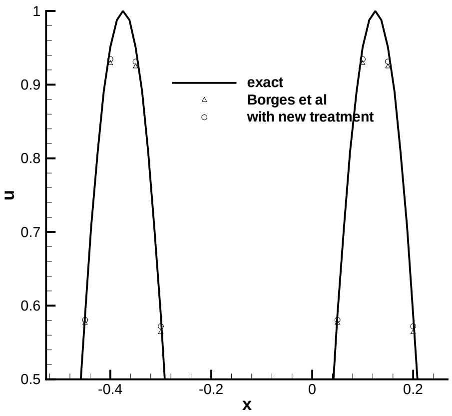

Figure 6: Results of the initial solution case 3 at $t = 1$, $N = 40$

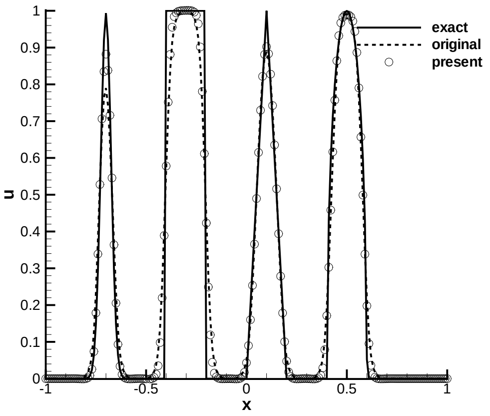

Figure 7: Results of the initial solution case 4 at $t = 4$, N=200

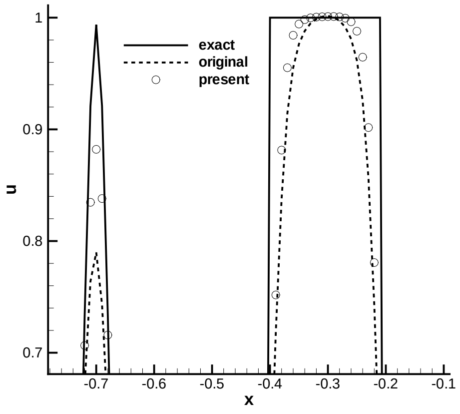

Figure 8: Locally enlarged plot of Fig. 7

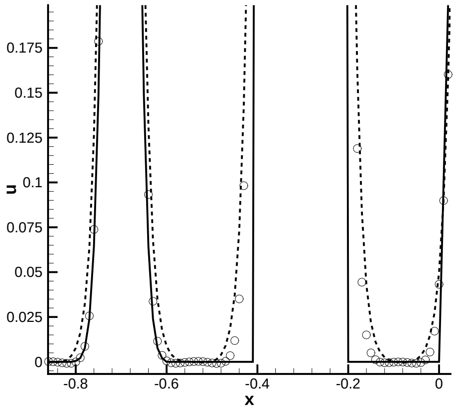

Figure 9: Locally enlarged plot of Fig. 7

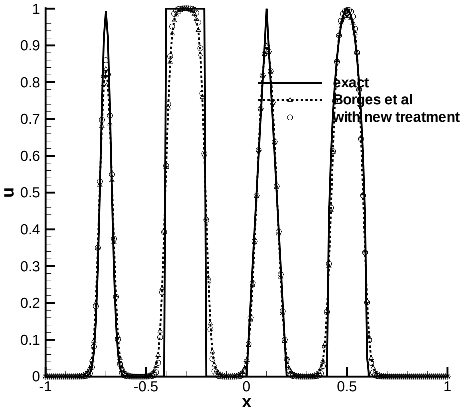

Figure 10: Results of the initial solution case 4 at $t = 8$, N=200

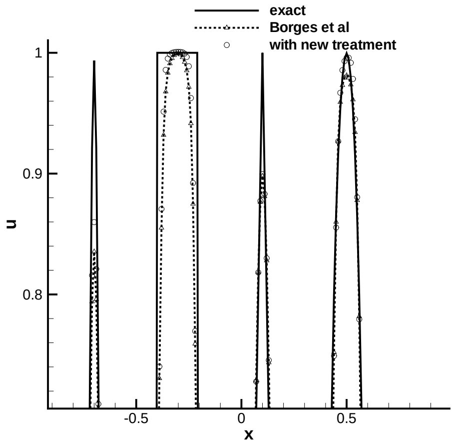

Figure 11: Locally enlarged plot of Fig. 10

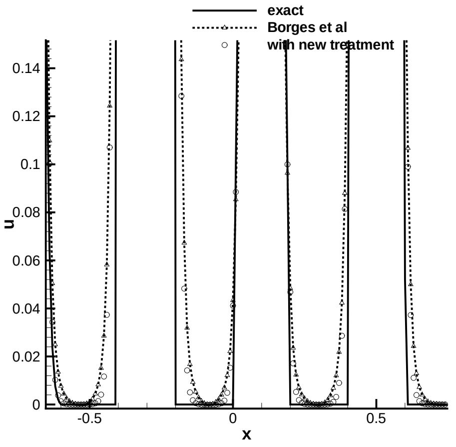

Figure 12: Locally enlarged plot of Fig. 10

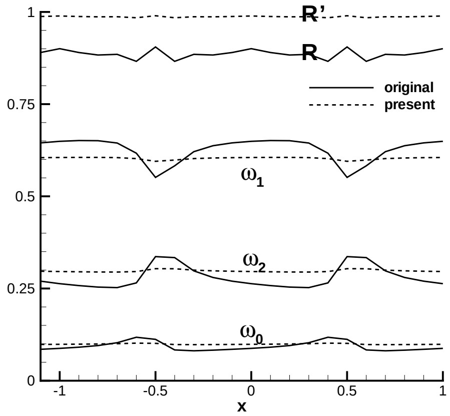

Figure 13: Comparison of ω_k and $Ratio = min(IS_0, IS_1, IS_2)/max(IS_0, IS_1, IS_2)$ of $sin(\pi x)$, N=20

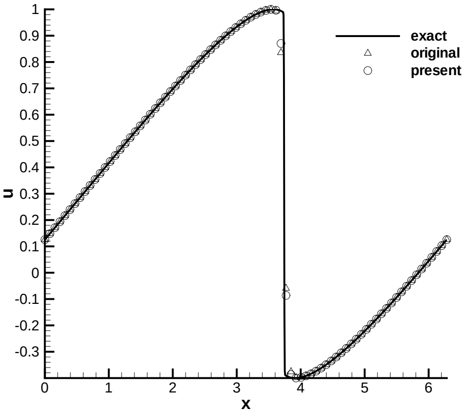

Figure 14: Nonlinear Transport Equation

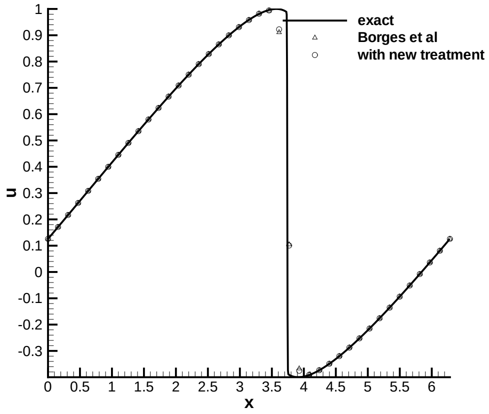

Figure 15: Nonlinear Transport Equation, $N = 40$

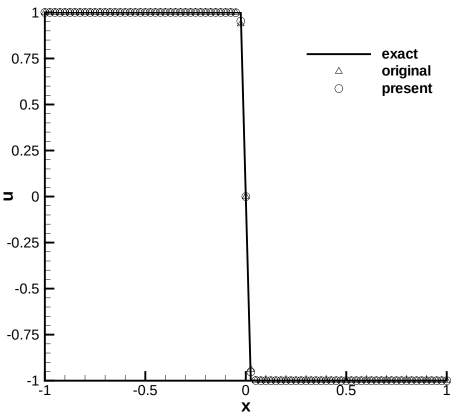

Figure 16: Viscous Burgers equation

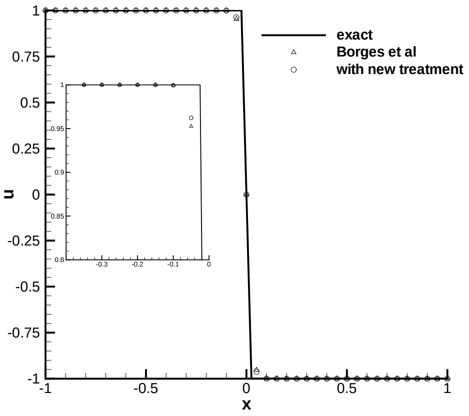

Figure 17: Viscous Burgers equation, $N = 40$

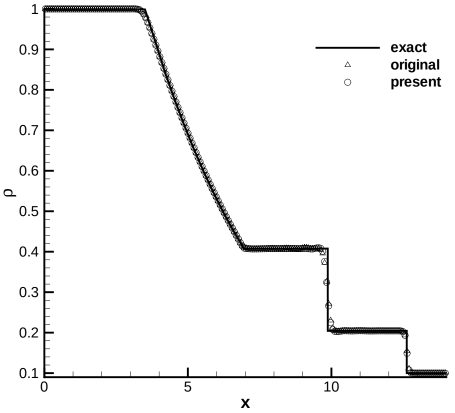

Figure 18: Density, Sod problem

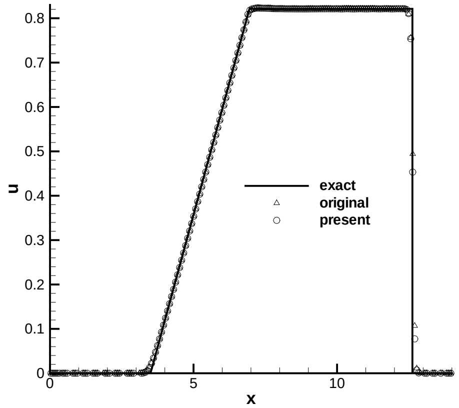

Figure 19: Velocity, Sod problem

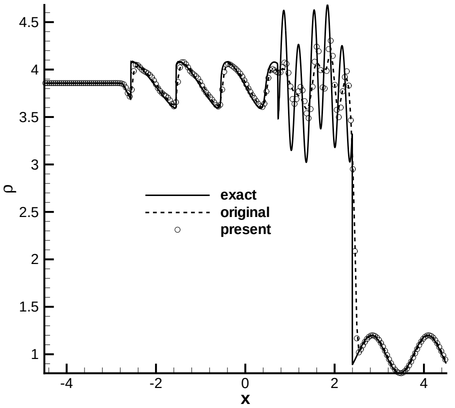

Figure 20: Density, Shu-Osher problem

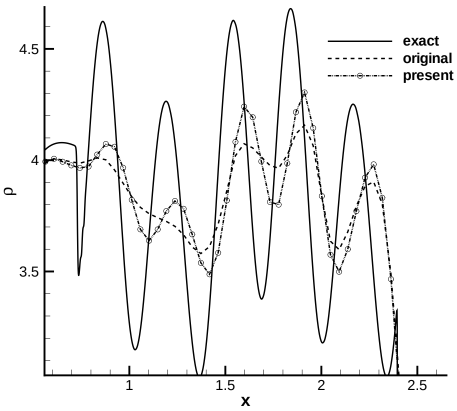

Figure 21: Locally enlarged plot of Fig. 20, Shu-Osher problem

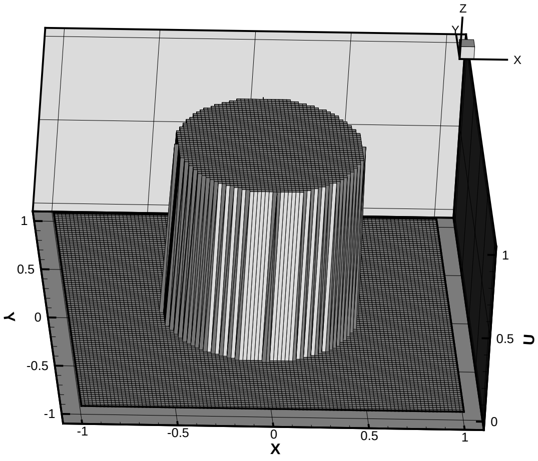

Figure 22: The initial distribution

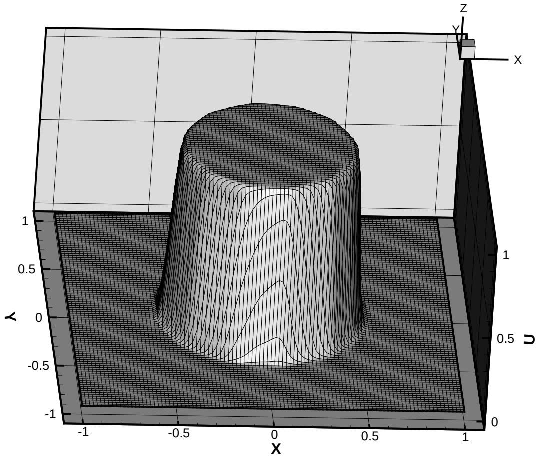

Figure 23: The results of the present WENO scheme

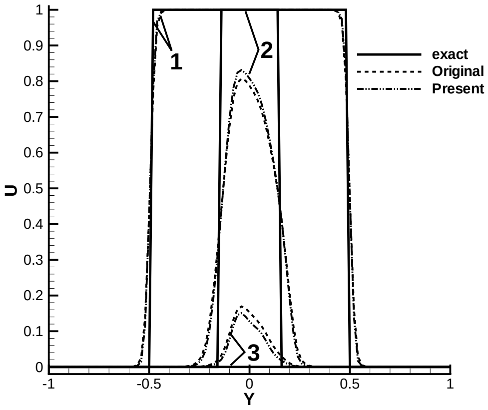

Figure 24: Comparison of results on lines. 1: $x = -0.02$; 2: $x = -0.48$; and 3: $x = -0.52$

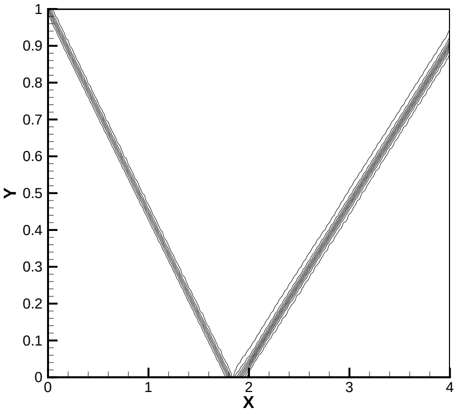

Figure 25: The pressure contours of the present WENO scheme

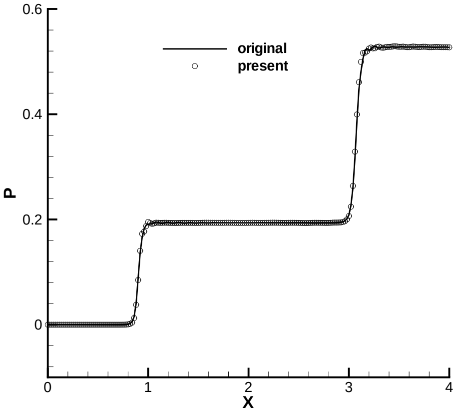

Figure 26: Comparison of pressure at the central line of y-direction

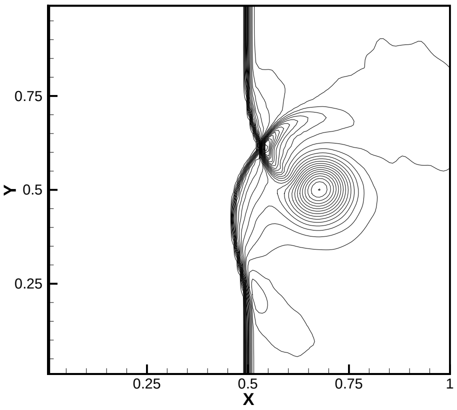

Figure 27: The pressure contours of present WENO scheme, $t = 0.35$

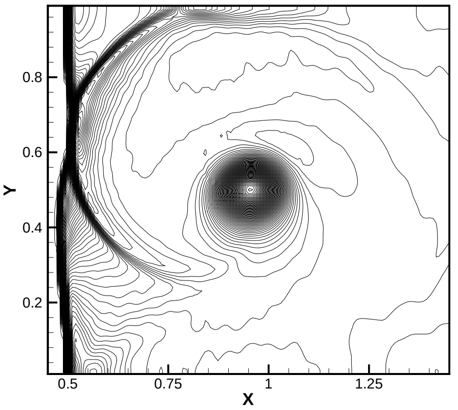

Figure 28: The pressure contours of present WENO scheme, $t = 0.60$

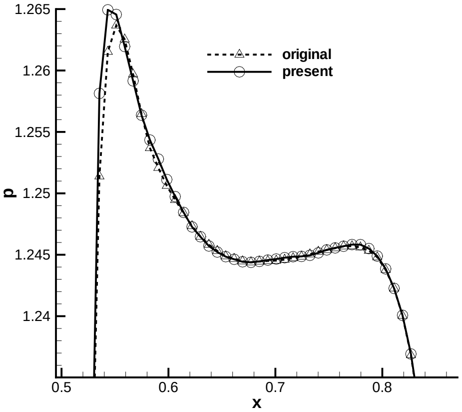

Figure 29: Comparison of pressure at the central line downstream the shock, $t = 0.60$

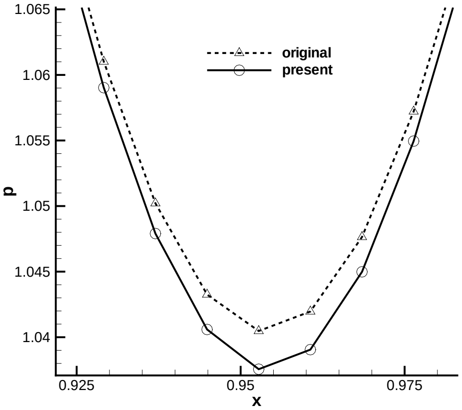

Figure 30: Comparison of pressure at the central line cross the vortex, $t = 0.60$